

experimental technique to study the motion of the AFM vector. Thus the dynamics of the AFM moment can be influenced and detected with an all-optical pump–probe method. In contrast to a ferromagnet, the AFM spins can be fully reoriented within a few picoseconds' time. This observation of the ultrafast orientation dynamics of the AFM moment may have far-reaching consequences for future spintronic devices. □

Methods

The measurements were performed in a pump and probe configuration at a photon energy of 1.55 eV using amplified pulses from a Ti:sapphire laser at a repetition rate of 1 kHz. Each pulse had an energy of about 2 μJ and a profile close to gaussian, with a width at half-maximum of about 100 fs. The sample (a 60-μm-thick TmFeO₃ single crystal cut perpendicular to the z axis) was placed in a cold finger cryostat where its temperature could be stabilized in the range of 10–300 K with a precision better than 0.5 K. The pump and probe beams were linearly polarized with an intensity ratio of about 100. Both beams were focused on the sample to a spot diameter of 50 μm at half maximum for the pump and somewhat smaller for the probe beam. The probe, polarized at 45° with respect to the y axis in the sample plane, detected the birefringence changes induced by the pump, using a sensitive two-diode balanced detection scheme.

Received 30 December 2003; accepted 17 May 2004; doi:10.1038/nature02659.

- Weiss, P. L'hypothèse du champ moléculaire et la propriété ferromagnétique. (The hypothesis of the molecular field and the property of ferromagnetism.). *J. Phys. Rad.* **6**, 661–669 (1907).
- Stoner, E. C. *Magnetism and Matter* (Methuen, London, 1934).
- Néel, L. Propriétés magnétiques de l'état métallique et énergie d'interaction entre atomes magnétiques. *Ann. Phys. (5e Ser.)* **5**, 232–237 (1936).
- Jubiläum issue. *J. Magn. Magn. Mater.* **200**, 1–789 (1999).
- Roukes, M. L. Electronics in a spin. *Nature* **411**, 747–748 (2001).
- Landau, L. D. & Lifshitz, E. M. *Electrodynamics of Continuous Media* (Pergamon, Oxford, 1960).
- Vonsovskii, S. V. *Magnetism* (John Wiley & Sons, New York, 1974).
- Gerrits, Th., van den Berg, H. A. M., Hohlfeld, J., Bär, L. & Rasing, Th. Ultrafast precessional magnetization reversal by picosecond magnetic field pulse shaping. *Nature* **418**, 509–512 (2002).
- Schumacher, H. W. *et al.* Phase coherent precessional magnetization reversal in microscopic spin valve elements. *Phys. Rev. Lett.* **90**, 017201 (2003).
- Schumacher, H. W., Chappert, C., Sousa, R. C., Freitas, P. P. & Miltat, J. Quasiballistic magnetization reversal. *Phys. Rev. Lett.* **90**, 017204 (2003).
- van Kampen, M. *et al.* All-optical probe of coherent spin waves. *Phys. Rev. Lett.* **88**, 227201 (2002).
- Ju, G. *et al.* Ultrafast time resolved photoinduced magnetization rotation in a ferromagnetic/antiferromagnetic exchange coupled system. *Phys. Rev. Lett.* **82**, 3705–3708 (1999).
- Skumryev, V. *et al.* Beating the superparamagnetic limit with exchange bias. *Nature* **423**, 850–853 (2003).
- Kittel, C. Theory of antiferromagnetic resonance. *Phys. Rev.* **82**, 565 (1951).
- Ney, O., Trzeciacki, M. & Hübner, W. Femtosecond dynamics of spin-dependent SHG response from NiO(001). *Appl. Phys. B* **74**, 741–744 (2002).
- Ferré, J. & Gehring, G. A. Linear optical birefringence of magnetic crystals. *Rep. Prog. Phys.* **47**, 513–611 (1984).
- White, R. L. Review of recent work on the magnetic and spectroscopic properties of the rare-earth orthoferrites. *J. Appl. Phys.* **40**, 1061–1069 (1969).
- Burzo, E. (ed.) *Numerical Data and Functional Relationships* Landolt-Börnstein New Series, Group III, Vol. 27f, 200–273 (Springer, Berlin, 1996).
- Hornor, H. & Varma, C. M. Nature of spin-reorientation transitions. *Phys. Rev. Lett.* **20**, 845–846 (1968).
- Shapiro, S. M., Axe, J. D. & Remeika, J. P. Neutron-scattering studies of spin waves in rare-earth orthoferrites. *Phys. Rev. B* **10**, 2014–2021 (1974).
- Koster, G. F., Dimmock, J. O., Wheeler, R. G. & Statz, H. *Properties of the Thirty-Two Point Groups* (MIT Press, Cambridge, Massachusetts, 1963).
- Belov, K. P., Volkov, R. A., Goranskii, B. P., Kadomtseva, A. M. & Uskov, V. V. Nature of the transitions during the spontaneous reorientation of spins in rare-earth orthoferrites. *Fiz. Tverd. Tela* **11**, 1148–1151 (1969); *Sov. Phys. Solid State* **11**, 935–938 (1969).
- Kimel, A. V., Pisarev, R. V., Bentivegna, F. & Rasing, Th. Time-resolved nonlinear optical spectroscopy of Mn³⁺ ions in rare-earth hexagonal manganites RMnO₃ (R = Sc, Y, Er). *Phys. Rev. B* **64**, 201103 (2001).
- Landau, L. D. & Lifshitz, E. M. On the theory of the dispersion of magnetic permeability in ferromagnetic bodies. *Phys. Zeit. Sowjetunion* **8**, 153–169 (1935).
- Andreev, A. F. & Marchenko, V. I. Symmetry and the macroscopic dynamics of magnetic materials. *Usp. Fiz. Nauk.* **130**, 39–63 (1980); *Sov. Phys. Usp.* **23**, 21–34 (1980).
- Kimel, A. V., Pisarev, R. V., Hohlfeld, J. & Rasing, T. H. Ultrafast quenching of the antiferromagnetic order in FeBO₃: Direct optical probing of the phonon-magnon coupling. *Phys. Rev. Lett.* **89**, 287401 (2002).
- Yosida, K. *Theory of Magnetism* 125–143 (Springer, Berlin, 1998).

Acknowledgements This work was partially supported by the European IST network SPINOSA, the RTN network DYNAMICS, the Russian Foundation for Basic Research and Stichting voor Fundamenteel Onderzoek der Materie (FOM).

Competing interests statement The authors declare that they have no competing financial interests.

Correspondence and requests for materials should be addressed to Th.R. (th.rasing@sci.kun.nl).

Reduction of hysteresis losses in the magnetic refrigerant Gd₅Ge₂Si₂ by the addition of iron

Virgil Provenzano*, Alexander J. Shapiro* & Robert D. Shull*

Magnetic Materials Group, NIST, 100 Bureau Drive, MS-8552, Gaithersburg, Maryland 20899, USA

* These authors contributed equally to this work

The magnetocaloric effect is the change in temperature of a material as a result of the alignment of its magnetic spins that occurs on exposure to an external magnetic field. The phenomenon forms the basis for magnetic refrigeration, a concept purported to be more efficient and environmentally friendly than conventional refrigeration systems^{1–5}. In 1997, a 'giant' magnetocaloric effect, between 270 K and 300 K, was reported in Gd₅Ge₂Si₂, demonstrating its potential as a near-room-temperature magnetic refrigerant^{6–8}. However, large hysteretic losses (which make magnetic refrigeration less efficient) occur in the same temperature range^{8,9}. Here we report the reduction (by more than 90 per cent) of these hysteretic losses by alloying the compound with a small amount of iron. This has the additional benefit of shifting the magnetic entropy change peak (a measure of the refrigerator's optimal operating temperature) from 275 K to 305 K, and broadening its width. Although the addition of iron does not significantly affect the refrigerant capacity of the material, a greater net capacity is obtained for the iron-containing alloy when the hysteresis losses are accounted for. The iron-containing alloy is thus a much-improved magnetic refrigerant for near-room-temperature applications.

The magnitude of the magnetocaloric effect is given by the field-induced entropy change, ΔS_m; that is, when a magnetic field is applied to the material there is a decrease in its magnetic entropy due to the alignment of the spins with the field. The reduction in the magnetic entropy is compensated by an increase in the lattice entropy of the system (via the creation of phonons), resulting in a temperature increase. The reverse takes place upon the removal of the applied field. This excursion in temperature, ΔT, is the basis for magnetic refrigeration.

It is now fairly well accepted that the mechanism behind the large magnetocaloric effect in Gd₅Ge₂Si₂ involves a magnetic-field-induced crystallographic structural change from the high-temperature monoclinic paramagnetic phase to the low-temperature orthorhombic ferromagnetic phase^{8,10–12}. Because of the coincidence of sizeable hysteretic losses and large magnetocaloric effects in the same temperature range, it is reasonable to conclude that the same mechanism is responsible for both phenomena. Here we report a method for suppressing the crystallographic phase change and thereby greatly reducing the hysteresis losses in the Gd₅Ge₂Si₂ compound.

Figure 1 compares the X-ray powder diffraction patterns of Gd₅Ge₂Si₂ (trace I) and Gd₅Ge_{1.9}Si₂Fe_{0.1} (trace II) alloy samples that were homogenized in vacuum at 1,300 °C (1,573 K) for 1 h; on the top left of Fig. 1 are presented backscattered scanning electron microscopy (SEM) micrographs showing the typical microstructure of the two alloys. The X-ray diffraction patterns show that although very similar, the two spectra are slightly shifted along the abscissa with respect to each other, and most of the peaks of both materials match quite closely those of the monoclinic phase structure^{11–13}. The notable differences between the two patterns are the increased magnitude in the iron-containing alloy of the peak centred around 35° and the appearance of some smaller peaks (centred at about 30°,

31.6° and 35.6°) in the $Gd_5Ge_{1.9}Si_2Fe_{0.1}$ alloy which are not present in the $Gd_5Ge_2Si_2$ spectrum. These differences in the two X-ray spectra are due to the microstructural differences in the two alloys (see discussion below). In fact, as it can be seen from the SEM micrographs, the $Gd_5Ge_2Si_2$ compound is observed to be single-phase (Fig. 1, left inset), whereas the microstructure of the alloy with the iron addition (Fig. 1, middle inset) is characterized by a dominant matrix (light grey) phase and by a minor (darker) phase located along the grain boundaries of the matrix phase. Closer examination of the smaller grain boundary phase in the iron-containing alloy shows it to be actually made up of two phases: a dark grey phase and a black phase (Fig. 1, right inset).

Energy-dispersive spectroscopy (EDS) analysis conducted on the two alloys yielded the following results. The composition, in atomic fraction, of the $Gd_5Ge_2Si_2$ compound was found to be 55% Gd, 22.6% Ge and 22.4% Si; these compositional values are very close to those obtained on the same alloy by a wet chemistry method, and are also close to the target composition of 55.6% Gd, 22.2% Ge and 22.2% Si. By contrast, the compositional values of the three phases present in the compound containing iron are as follows: (1) for the dominant matrix phase — 60% Gd, 22.2% Ge, 17.8% Si and no iron; (2) for the lighter grain boundary phase — 35.3% Gd, 11.2% Ge, 25.6% Si and 27.9% Fe; (3) for the darker grain boundary phase — 22.2% Gd, 7.2% Ge, 34.4% Si and 36.2% Fe. Note that the dominant phase in the iron-containing compound had a larger content of both Gd and Ge and a smaller concentration of Si relative to the target composition of 55.6% Gd, 21.1% Ge, 22.2% Si and 1.1% Fe. On the other hand, the grain boundary phases were both rich in Si and Fe. These results strongly suggest that one of the major effects of the iron addition is for it to combine primarily with the silicon (giving rise to the two boundary phases), resulting in a matrix phase that is depleted in silicon compared to the single phase of the alloy without iron. The greater concentration of Gd, together with the

deficiency of Si in the matrix phase, probably plays a pivotal role in the different magnetic behaviour of the $Gd_5Ge_{1.9}Si_2Fe_{0.1}$ alloy, compared to that of the compound without iron.

The two sets of hysteresis loops presented in Fig. 2 illustrate the hysteresis losses for the two alloys in the 260–320 K temperature range. In this temperature interval the $Gd_5Ge_2Si_2$ compound exhibits large hysteretic losses (Fig. 2a), coinciding with the same temperature interval in which the corresponding magnetic entropy change, ΔS_m , attains its peak values. A summary of hysteretic loss values over the temperature range of interest is presented in Fig. 3. These hysteretic losses were determined by computing the hatched area inside each magnetization (M) versus field (H) loop shown in Fig. 2. It can be seen clearly that the addition of about one atomic per cent of iron to the alloy resulted in a reduction of the hysteresis losses by nearly 95 per cent when compared to the alloy without the iron addition.

Closer examination of the M – H loops shown in Fig. 2 provides additional insight concerning the effect of the iron addition on the magnetocaloric response of the $Gd_5Ge_2Si_2$ compound in the 270–320 K temperature range. For the alloy without the iron addition (Fig. 2a), the magnetization measured in the first half of the loop shows a distinct magnetic transition with increasing field between 270 K and 290 K; this transition occurs at higher field values with increasing temperature. As already stated, it has been hypothesized that this transition is the result of a field-induced first-order crystallographic phase change from the paramagnetic monoclinic phase to a ferromagnetic orthorhombic phase^{8,10–12}. The M – H loops clearly show that this field-induced phase transition reverses upon decreasing the field, but with some hysteresis in the transition field. Below 270 K this alloy exhibits ferromagnetic behaviour, whereas above 295 K the material is paramagnetic.

By contrast, the M – H loops of the $Gd_5Ge_{1.9}Si_2Fe_{0.1}$ alloy (Fig. 2b) do not show any field-induced magnetic transition in the 260–340 K

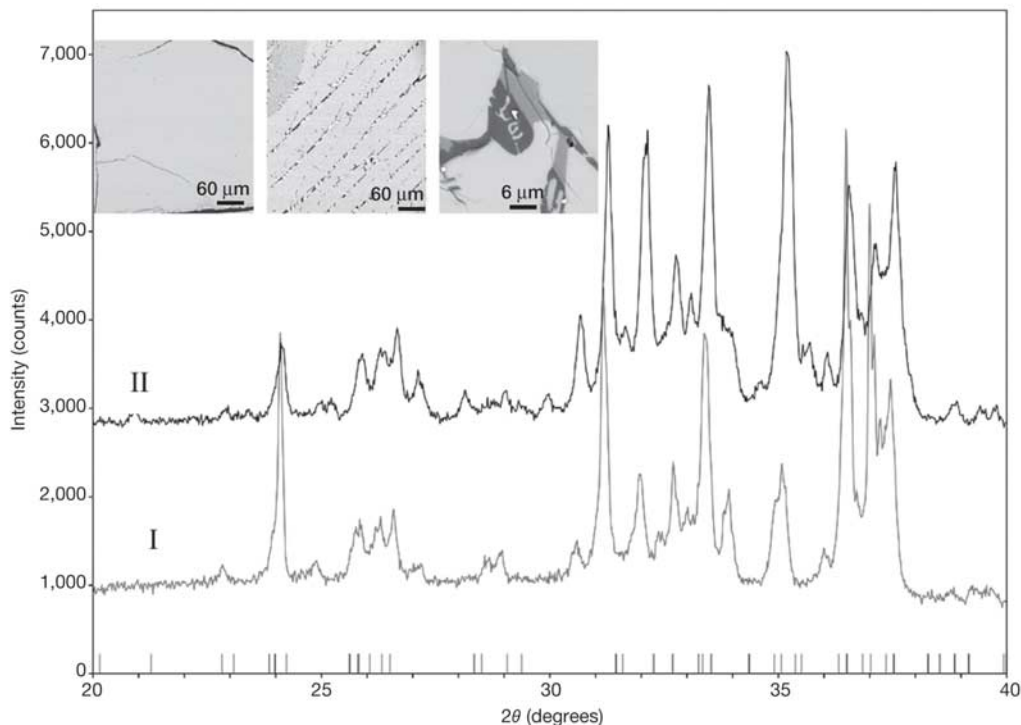


Figure 1 X-ray diffraction spectra and SEM micrographs of the two alloys. Cu-K α X-ray diffraction spectra measured at room temperature for the $Gd_5Ge_2Si_2$ compound (I) and the $Gd_5Ge_{1.9}Si_2Fe_{0.1}$ alloy (II). The Bragg peak positions for the monoclinic phase are shown along the x-axis. Insets, backscattered SEM micrographs, showing typical microstructures

of the $Gd_5Ge_2Si_2$ (left inset) and $Gd_5Ge_{1.9}Si_2Fe_{0.1}$ (middle and right inset) alloys; $Gd_5Ge_2Si_2$ is single phase, whereas the $Gd_5Ge_{1.9}Si_2Fe_{0.1}$ alloy consists of a dominant grey phase and a minor, darker intergranular phase.

temperature range. In fact, here the magnetic data show a gradual shift from ferromagnetic behaviour to superparamagnetic behaviour, as evidenced by the appearance of curvature in the M - H plots with increasing T ; above 320 K, the material is paramagnetic. By comparison, the $\text{Gd}_5\text{Ge}_2\text{Si}_2$ compound exhibits paramagnetic behaviour at temperatures above 290 K. Although not shown here, the M versus T data of the $\text{Gd}_5\text{Ge}_{1.9}\text{Si}_2\text{Fe}_{0.1}$ alloy at $H = 796 \text{ kA m}^{-1}$ (1 T) exhibit no magnetic transition for temperatures below 260 K. The X-ray diffraction data (Fig. 1) and the magnetization data (Fig. 2) strongly suggest that the main effect of the iron addition in the $\text{Gd}_5\text{Ge}_2\text{Si}_2$ compound is to suppress the field-induced monoclinic-to-orthorhombic phase transition in the 270–320 K range, resulting in much smaller hysteresis losses. This field-induced phase transition is absent in the iron-containing alloy because the orthorhombic phase never forms for $H < 3,980 \text{ kA m}^{-1}$ (5 T) between 10 K and 360 K, whereas it does form in $\text{Gd}_5\text{Ge}_2\text{Si}_2$ at $T < 270 \text{ K}$ without the presence of a magnetic field.

Variation of the magnetic entropy change, ΔS_m , with temperature for the two alloys is shown in Fig. 4. These data were computed from the isothermal M - H data of the two alloys using equation (3). For the alloy without iron, the value of the ΔS_m peak, integrated over an applied field $\Delta H = 3,980 \text{ kA m}^{-1}$ (5 T), is about a factor of 3

higher than that for the alloy with the iron ($20 \text{ J kg}^{-1} \text{ K}^{-1}$ versus $7 \text{ J kg}^{-1} \text{ K}^{-1}$, respectively). However, the ΔS_m peak width of the iron-containing alloy is considerably broader. For this latter alloy, the peak of ΔS_m occurs at about 305 K (Fig. 4b), whereas in the alloy without iron, the ΔS_m peak occurs nears 275 K (Fig. 4a). From the data presented in Fig. 4, the refrigerant capacity (RC) value was computed for the two alloys for $\Delta H = 3,980 \text{ kA m}^{-1}$ (5 T), using the two approaches described in the Methods section. The RC values computed by the expression given in ref. 14 were respectively around 360 J kg^{-1} and 305 J kg^{-1} for the alloys with and without the iron addition, whereas the RC values computed by the Wood and Potter method¹⁵ were respectively around 240 J kg^{-1} and 265 J kg^{-1} .

In the temperature ranges where the RC values were computed by both methods, the average hysteretic loss is about 65 J kg^{-1} for the compound without iron but less than 4 J kg^{-1} for the compound with the iron addition. Because these are the costs in energy to make one cycle of the magnetic field, they must be considered when calculating the usefulness of a magnetic refrigerant being subjected to cyclic fields. One way to take into account the hysteresis loss of each alloy is to simply subtract it from the corresponding RC value. Subtraction of the average hysteresis for each alloy from the corresponding RC values computed by the methods of refs 14 and 15 respectively yielded approximate values of 355 J kg^{-1} and 235 J kg^{-1} for the Fe-containing alloy, and approximate values of 240 J kg^{-1} and 200 J kg^{-1} for the alloy without the Fe addition. Note how much larger are the resultant values for the Fe-containing alloy regardless of the RC calculation method. Therefore, on this basis the $\text{Gd}_5\text{Ge}_{1.9}\text{Si}_2\text{Fe}_{0.1}$ alloy is a much better magnetic refrigerant than the $\text{Gd}_5\text{Ge}_2\text{Si}_2$ compound despite its lower ΔS_m peak value.

In order to examine further the effect of iron concentration on the magnetic properties of the $\text{Gd}_5\text{Ge}_2\text{Si}_2$ compound, especially with regard to the hysteretic losses, two additional alloy samples were prepared. These alloys had respectively one-half and twice the iron concentration of $\text{Gd}_5\text{Ge}_{1.9}\text{Si}_2\text{Fe}_{0.1}$; they were arc-melted and homogenized as described in the Methods section for the other two alloys. Owing to space limitations, details of their microstructure and magnetic data are not presented here, but their magnetic properties can be summarized as follows. For the alloy having half the iron concentration, the M - H loops were similar to those of the $\text{Gd}_5\text{Ge}_2\text{Si}_2$ compound—that is, they showed the presence of both large hysteresis losses and a field-induced magnetic phase transition in the 260–320 K temperature range. However, compared to the iron-free compound, the hysteresis losses were only about 50% smaller and the field-induced phase transition was less pronounced. The M - H loops of the alloy having twice the iron concentration had

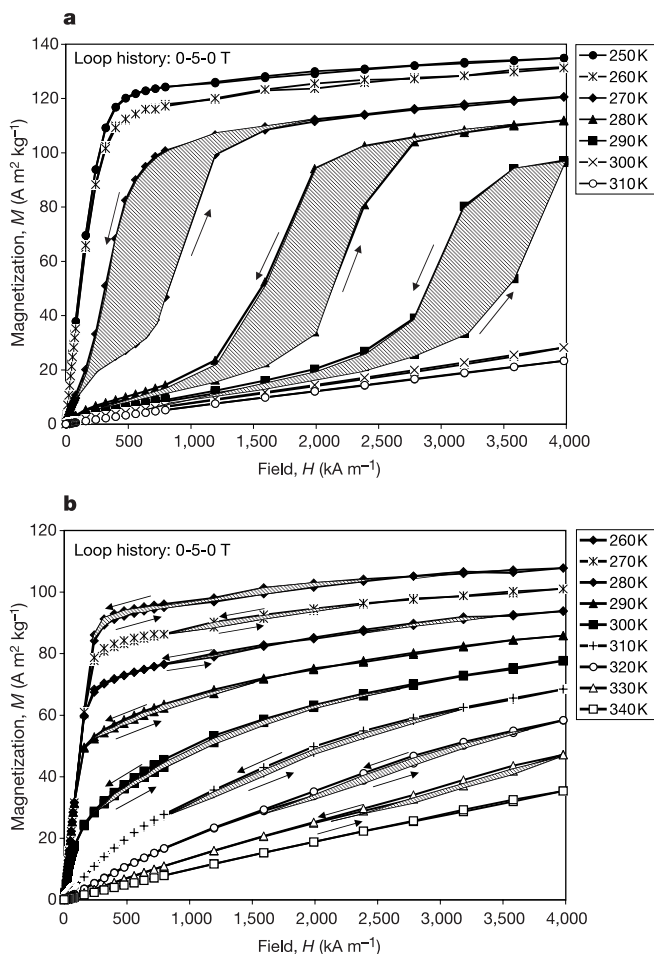


Figure 2 Magnetization versus field curves. Magnetization versus field curves for the $\text{Gd}_5\text{Ge}_2\text{Si}_2$ compound between 250 K and 310 K (a) and for the $\text{Gd}_5\text{Ge}_{1.9}\text{Si}_2\text{Fe}_{0.1}$ alloy between 260 K and 340 K (b); arrows indicate the sequence of measurements. The curves qualitatively illustrate the large hysteresis losses of the $\text{Gd}_5\text{Ge}_2\text{Si}_2$ compound and the much smaller values of the $\text{Gd}_5\text{Ge}_{1.9}\text{Si}_2\text{Fe}_{0.1}$ alloy. In addition, paramagnetic behaviour is observed above the different temperatures 320 K and 290 K for the Fe-containing alloy and $\text{Gd}_5\text{Ge}_2\text{Si}_2$ compound, respectively.

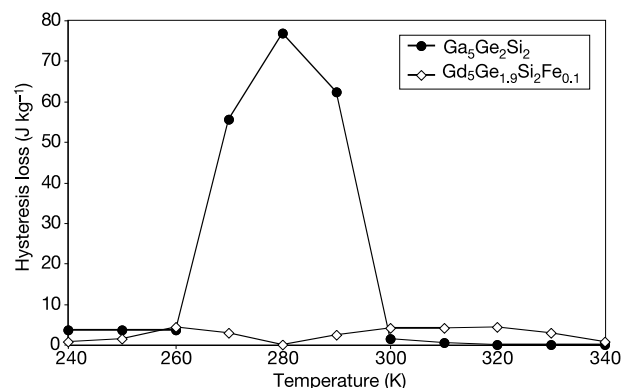


Figure 3 Comparison of hysteresis losses. Comparison of hysteresis losses (calculated as described in the text) of the $\text{Gd}_5\text{Ge}_2\text{Si}_2$ (filled circles) and $\text{Gd}_5\text{Ge}_{1.9}\text{Si}_2\text{Fe}_{0.1}$ (open diamonds) alloys plotted as a function of temperature.

almost double the hysteresis losses of the $\text{Gd}_5\text{Ge}_{1.9}\text{Si}_2\text{Fe}_{0.1}$ alloy, and there was a slight indication of a field-induced phase transition in the 260–320 K temperature range. These results show a systematic variation of magnetic character with iron concentration, and show that the lowest hysteresis losses were observed for the alloy whose iron concentration was about 1 per cent atomic fraction.

As mentioned earlier, one of the major effects of the iron addition to the $\text{Gd}_5\text{Ge}_2\text{Si}_2$ compound is to suppress the formation of the orthorhombic phase. In the $\text{Gd}_5\text{Ge}_{1.9}\text{Si}_2\text{Fe}_{0.1}$ alloy, the monoclinic phase is the stable structure even at low temperatures, and the amount of orthorhombic phase that forms is quite small. In $\text{Gd}_5\text{Ge}_2\text{Si}_2$ the stable structure is the orthorhombic phase below 270 K and the monoclinic phase above 270 K. Therefore, as the amount of orthorhombic phase is very small in the iron-containing alloy, the monoclinic-to-orthorhombic field-induced phase transformation is not observed between 260 K and 340 K for H application up to $3,980 \text{ kA m}^{-1}$ (5 T), resulting in negligible hysteretic losses. The reverse is true for the alloy without the iron addition. This change in thermodynamics is probably related to the reduction in Si content and the increase in Gd content of the matrix phase when iron is added to the $\text{Gd}_5\text{Ge}_2\text{Si}_2$ compound. The multiple-phase nature of the quaternary alloy probably also contributes to the stabilization of the monoclinic structure, perhaps by mediating the compressive stress created during cooling as the alloy contracts.

The Fe addition also creates a magnetic nanostructure. The

superparamagnetic behaviour observed in the $\text{Gd}_5\text{Ge}_{1.9}\text{Si}_2\text{Fe}_{0.1}$ quaternary alloy (and not in the $\text{Gd}_5\text{Ge}_2\text{Si}_2$ compound) at higher temperatures shows that the ferromagnetic matrix phase has been broken up into nanometre-sized ferromagnetic clusters. This type of magnetic nanocomposite morphology has been shown to lead to enhanced magnetocaloric effects^{4,16,17}, and is probably also the reason why the ΔS_m peak width of the iron-containing alloy is considerably broader. How such a magnetic structure developed is unknown. Certainly the microstructure does not show this nano-scale structure, so the cause must be more subtle (perhaps the inhomogeneous distribution of vacancies or defects in the Gd-Si-Ge matrix phase). □

Methods

The samples used in this study were prepared by arc melting, using a water-cooled copper hearth in an argon atmosphere under ambient pressure starting with the appropriate amounts of the component elements. The compound without the iron addition was prepared by the Materials Preparation Centre of the Ames Laboratory, Ames, Iowa, whereas the alloy with the iron addition was prepared at the alloy melting facility of the American Dental Association at NIST. The purity of the starting constituents was 99.9% mass fraction or better for the two alloys; and their target compositions were as follows: $\text{Gd}_5\text{Ge}_2\text{Si}_2$ and $\text{Gd}_5\text{Ge}_{1.9}\text{Si}_2\text{Fe}_{0.1}$ (approximately one atomic per cent Fe). Before making magnetic measurements, the alloy samples were homogenized at $1,300^\circ\text{C}$ for one hour in vacuum⁷. Following the homogenizing treatment, the crystal structure and the microstructure of the samples were respectively characterized by Cu-K α powder X-ray diffraction (XRD) analysis, and by SEM and EDS. The magnetocaloric effect of the two alloys were determined by measuring M as a function of T and H , using a SQUID magnetometer. The magnetometer, calibrated by a pure Ni sphere SRM no. 772 from NIST, was programmed to measure M at discrete magnetic field values between 0 and $3,980 \text{ kA m}^{-1}$ (5 T) while the temperature was held constant. Then the measurement sequence was repeated many times successively at each 10 K interval as the temperature was raised from 10 K up to 360 K. The M values were normalized by dividing them by the corresponding sample mass. ΔS_m was then calculated from the M data using the integrated Maxwell relation:

$$\left(\frac{\partial S}{\partial H}\right)_T = \left(\frac{\partial M}{\partial T}\right)_H \tag{1}$$

Integration of the above expression leads to:

$$\Delta S_m(T, \Delta S) = \int_0^{H'} \left(\frac{\partial M}{\partial T}\right)_H dH \tag{2}$$

For M measurements made at constant temperature at discrete H intervals, the above Maxwell expression can be approximated by the following expression:

$$\Delta S_m \approx \frac{1}{\Delta T} \left[\int_0^{H'} M(T + \Delta T, H) dH - \int_0^{H'} M(T, H) dH \right] \tag{3}$$

Therefore, using the approximation given by equation (3), ΔS_m as a function of temperature for each sample was computed numerically by first differentiating the magnetization data, M , with respect to temperature, and then integrating the resulting derivatives from zero field to some value H up to 5 T.

We now discuss the experimental uncertainty in the measurements of H , T and M that directly affect the overall accuracy of the ΔS_m values computed by equation (3). Values of H between zero and $3,980 \text{ kA m}^{-1}$ (5 T) are known to within 0.2%. During each set of isothermal magnetic measurements where M was measured as a function of magnetic field, the temperature was kept constant to within 0.02 K. Accuracy of the magnetization data varied from 0.5% to 2% for both alloys, with most data having an uncertainty of less than 1% at non-zero field values. At zero field, the uncertainty ranged from 1% to 8%. Consequently, the error in ΔS_m is about 1% or less. We represent these errors by the sizes of the symbols in Figs 2–4. In Fig. 4b, below 250 K there is some oscillation in the ΔS_m versus T plot that is not a reflection of uncertainty in the data, but rather reflects real variations in the magnetization data, probably due to the secondary phases in the alloy. In fact, we prepared two alloys having compositions of the secondary phases detected in the Fe-containing alloy discussed here, and observed peaks in ΔS_m that correlate with the temperature regions of oscillation shown in Fig. 4b. These results will be presented elsewhere. Even though the data shown in Fig. 4 were calculated using measured M versus H data taken at 10 K intervals for comparison with earlier published data^{7,8}, the temperature of maximum ΔS_m was also computed from magnetic data measured at 4 K intervals, leading us to conclude that the temperature at which ΔS_m is maximum is accurate to within ± 5 K.

RC values for the two alloys were determined by two different methods. In the first method¹⁴, the RC values were obtained by numerically integrating the area (shaded in Fig. 4) under the ΔS_m versus T curves, using the temperatures at half-maximum of the ΔS_m peak as the integration limits. In the second method, the RC values were computed using the approach suggested by Wood and Potter¹⁵ and later used by other researchers in the field^{18,19}. Wood and Potter defined the refrigerant capacity for a reversible refrigeration cycle operating between T_h (the temperature of the hot reservoir) and T_c (the temperature of the cold reservoir) as $\text{RC} = \Delta S_m \Delta T$, where ΔS_m is the magnetic entropy change at the hot and cold ends of the cycle (defined equal) and $\Delta T = T_h - T_c$. According to this approach, for a given magnetic refrigerant the optimum refrigeration cycle occurs when

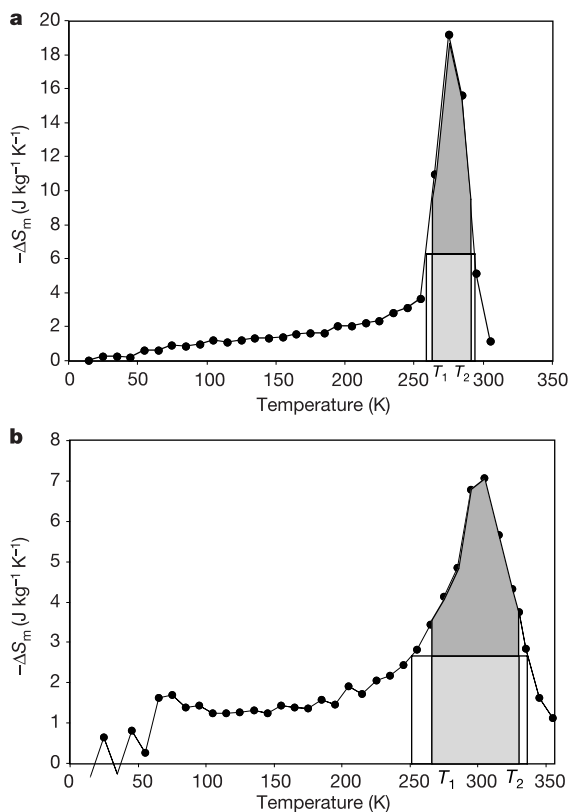


Figure 4 Computed ΔS_m and RC values. Computed ΔS_m (for $\Delta H = 3,980 \text{ kA m}^{-1}$ (5 T)), normalized with respect to sample mass, of the $\text{Gd}_5\text{Ge}_2\text{Si}_2$ compound (a) and of the $\text{Gd}_5\text{Ge}_{1.9}\text{Si}_2\text{Fe}_{0.1}$ alloy (b), plotted as a function of temperature. Note the presence of peaks centred near 270 K and 305 K respectively for the $\text{Gd}_5\text{Ge}_2\text{Si}_2$ compound and the $\text{Gd}_5\text{Ge}_{1.9}\text{Si}_2\text{Fe}_{0.1}$ alloy. The refrigerant capacities (RC), calculated as described in the Methods section, are also shown as the shaded areas and unshaded rectangles for each material; T_1 and T_2 refer to the limits of integration for calculating the shaded areas. Compared to the $\text{Gd}_5\text{Ge}_2\text{Si}_2$ compound, the iron-containing compound exhibits a broader ΔS_m peak and a ΔS_m peak at a higher temperature.

the quantity $\Delta S_m \Delta T$ is maximum. The RC values computed by the Wood and Potter method are shown in Fig. 4 as the rectangular areas overlapping and extending outside the shaded areas.

Received 2 December 2003; accepted 5 December 2004; doi:10.1038/nature02657.

- Glanz, J. Making a bigger chill with magnets. *Science* **279**, 2045 (1998).
- Tegus, O., Bruck, E., Buschow, K. H. J. & de Boer, F. R. Transition-metal-based refrigerants for room-temperature applications. *Nature* **415**, 150–152 (2002).
- Tegus, O. *et al.* Magnetic-phase transitions and magnetocaloric effects. *Physica B* **319**, 174–192 (2002).
- McMichael, R. D., Shull, R. D., Swartzendruber, L. J., Bennett, L. H. & Watson, R. E. Magnetocaloric effect in superparamagnets. *J. Magn. Magn. Mater* **111**, 29–33 (1992).
- Fujita, A., Fujieda, S., Hasegawa, Y. & Fukamichi, K. Itinerant-electron metamagnetic transition and large magnetocaloric effects. *Phys. Rev. B* **67**, 104416 (2003).
- Pecharsky, V. K. & Gschneidner, K. A. Jr The giant magnetocaloric effect in $Gd_5(Si_2Ge_2)$. *Phys. Rev. Lett.* **78**, 4494–4497 (1997).
- Pecharsky, A. O., Gschneidner, K. A. Jr & Pecharsky, V. K. The giant magnetocaloric effect of optimally prepared $G_5Ge_2Si_2$. *J. Appl. Phys.* **93**, 4722–4728 (2003).
- Levin, E. M., Pecharsky, V. K. & Gschneidner, K. A. Jr Unusual magnetic behavior in $G_5(Ge_{1.5}Si_{2.5})$ and $G_5Ge_2Si_2$. *Phys. Rev. B* **62**, R14625–R14628 (2000).
- Giguere, A. *et al.* Direct measurements of the 'giant' adiabatic temperature change in $G_5Ge_2Si_2$. *Phys. Rev. Lett.* **83**, 2262–2265 (1999).
- Choe, W. *et al.* Making and breaking covalent bonds across the magnetic transition in the giant magnetocaloric material $Gd_5(Ge_2Si_2)$. *Phys. Rev. Lett.* **84**, 4617–4620 (2000).
- Morellon, L., Algarabel, P. A., Ibarra, M. R., Blasco, J. & Garcia-Landa, B. Magnetic-field-induced structural transition in $Gd_5(Si_{1.8}Ge_{2.2})$. *Phys. Rev. B* **58**, R14721–R14724 (1998).
- Meyers, J., Chumbley, S., Choe, W. & Miller, G. J. Microstructural analysis of twinned β - $G_5Ge_2Si_2$. *Phys. Rev. B* **66**, 012106 (2002).
- Pecharsky, V. K. & Gschneidner, K. A. Jr Phase relationship and crystallography in pseudobinary system Gd_5Si_4 - Gd_5Ge_4 . *J. Alloys Compd.* **260**, 98–106 (1997).
- Gschneidner, K. A. Jr, Pecharsky, V. K., Pecharsky, A. O. & Zimm, C. B. Recent development in magnetic refrigeration. *Mater. Sci. Forum* **315–317**, 69–76 (1999).
- Wood, M. E. & Potter, W. H. General analysis of magnetic refrigeration and its optimization using a new concept: maximization of refrigerant capacity. *Cryogenics* **25**, 667–683 (1985).
- Shull, R. D., Swartzendruber, L. J. & Bennett, L. H. in *Proc. Sixth Int. Cryocoolers Conf.* (eds Green, G. & Knox, M.) 231 (Publication no. DTRC-91/002, David Taylor Research Center, Annapolis, Maryland, 1991).
- McMichael, R. D., Ritter, J. J. & Shull, R. D. Enhanced magnetocaloric effect in $Gd_5Ga_8Fe_xO_{12}$. *J. Appl. Phys.* **73**, 6946–6948 (1993).
- Tishin, A. M. Magnetic refrigeration in the low-temperature range. *J. Appl. Phys.* **68**, 6480–6484 (1990).
- von Ranke, P. J. *et al.* Anomalous magnetocaloric effect in YbAs associated with the giant quadrupolar interaction. *Phys. Rev. B* **63**, 24422 (2001).

Acknowledgements This work was partially supported by the NASA-Goddard Space Flight Center. We thank R. Waterstrat and R. Drew for technical assistance, and M. Lufaso and R. D. McMichael for helpful discussions.

Competing interests statement The authors declare that they have no competing financial interests.

Correspondence and requests for materials should be addressed to V.P. (virgil12@nist.gov).

Evidence for a macroscopic electric field in the sedimentation profiles of charged colloids

Mircea Raşa & Albert P. Philipse

Van 't Hoff Laboratory for Physical and Colloid Chemistry, Debye Institute, Utrecht University, Padualaan 8, 3584 CH Utrecht, The Netherlands

The determination of molecular masses from barometric sedimentation profiles, a main topic in ultracentrifugal analysis, is thought to be quantitatively correct for non-interacting particles^{1,2}. Whereas this expectation is justified for uncharged colloids or macromolecules at low volume fractions, early ultracentrifugation studies³ on charged particles had already indicated that the obtained masses might be much too low. More recently, expanded sedimentation profiles have been observed for charged particles^{4,5}, sometimes inflated by orders of magnitude⁵ relative to the barometric prediction, which highlights a short-

coming in our understanding of centrifugation of even very dilute charged species⁵. Theory⁶ and simulations⁷, anticipated by various authors^{4,8,9}, now propose that strongly non-barometric sedimentation profiles might be caused by an internal macroscopic electric field that, even for non-interacting particles, significantly decreases the buoyant particle mass. The existence of this field and its intriguing consequences still lack experimental verification. Here we report ultracentrifugation experiments on charged colloidal silica spheres, showing both the existence of such a macroscopic electric field and its drastic effects on the sedimentation profiles of very dilute dispersions at low ionic strength.

Centrifugation is an indispensable technique for separating and analysing cells, organelles and macromolecules^{1,2}, as well as colloids¹⁰. A classical example is the centrifugation of DNA fragments in salt gradients, which confirmed the Watson–Crick model for DNA replication^{11,12}. Absolute molecular masses can be determined directly under non-denaturing conditions from sedimentation–diffusion (SD) concentration profiles, a method reported to be rigorous². The method assumes that, for sedimentation under gravity, the particle number density $\rho(x)$ at an altitude x in the SD profile follows from a Boltzmann distribution and has the form

$$\ln(\rho(x)) \propto -x/L \quad (1)$$

In this 'barometric' profile, $L = k_B T / (mg)$ is the gravitational length for particles with buoyant mass m , T is the absolute temperature, k_B is the Boltzmann constant and g is the gravitational acceleration. It is generally assumed¹⁰ that non-interacting particles will adopt such a barometric profile and that, consequently, sufficiently low concentrations ensure the validity of equation (1). Here, however, we report SD profiles of very dilute charged colloids that strongly deviate from the barometric distribution (equation (1)) owing to an electric field, which has only recently^{6,7,13} been clearly identified as an important factor in the centrifugation of charged species.

Non-barometric behaviour due to an electric field is predicted to occur at sufficiently low ionic strength⁶, and therefore we have studied the ultracentrifugation of well-defined, charged silica spheres (Table 1) in ethanol. This solvent is suitable because of its inherent low ionic strength and its ability to disperse charged silica spheres to non-aggregated 'alcosols' with practically unlimited colloidal stability^{5,14,15}. We found that the centrifuged silica spheres form reproducible SD profiles that can be scanned with high spatial resolution (Fig. 1; see Methods section). SD profiles were studied for initial silica volume fractions down to 0.01% to minimize the effect of inter-particle interactions. We verified that the barometric part (region I; see below) of SD profiles yields a correct colloid radius: for a silica mass density of 1.6 g cm^{-3} (Table 1), the measured centrifugal lengths correspond to a radius of 19.2 nm, which lies within the radius distribution determined from electron microscopy (Table 1). We also verified that uncharged silica spheres dispersed in cyclohexane yield the expected barometric profiles. However, for charged silica spheres all our experimental SD profiles, with a representative selection in Fig. 1, deviate drastically from the barometric distribution.

These deviations are due to a macroscopic electric field in the SD profile, that is, a gradient in an equilibrium electrical potential,

Table 1 Properties of silica spheres (Labcode SIA) dispersed in ethanol

R (nm)	σ (%)	R_h (nm)	δ (g cm^{-3})	μ ($\mu\text{m cm V}^{-1} \text{ s}^{-1}$)	z
21.9	11.6	30.0	1.6 ± 0.1	-0.95 ± 0.05	≈ 50

R and σ are radius and polydispersity, respectively, from transmission electron microscopy; R_h is the radius from dynamic light scattering; δ is the mass density from ref. 14; μ is the electrophoretic mobility for silica volume fractions in the range 0.01–0.3%; z is the number of elementary charges on silica particles, determined from electrophoretic mobility. Errors are \pm s.d.